EUROPEAN FUSION DEVELOPMENT AGREEMENT

EFDA–JET–R(04)01

G.Bonheure, S. Popovichev, S. Conroy, L. Bertalot, A. Murariu,
and JET EFDA Contributors*

First Results on MeV Ion Losses Measurements based on Activation Techniques during Helium Plasma Experiments on JET with ICRF third Harmonic Heating of Helium Beam Ions

First Results on MeV ion Losses Measurements based on Activation Techniques during Helium Plasma Experiments on JET with ICRF third Harmonic Heating of Helium Beam Ions

G. Bonheure[1], S. Popovichev[2], S. Conroy[3], L. Bertalot[4], A. Murariu[5], and JET EFDA Contributors*

[1]Partners in the Trilateral Euregio Cluster, ERM-KMS, B 1000 Brussels, Belgium
[2]EURATOM/UKAEA Fusion Association, Culham Science Centre, Abingdon, Oxon, OX14 3DB UK
[3]EURATOM-VR Association, Uppsala, Sweden,
[4]Associazione EURATOM/ENEA sulla Fusione, Frascati, Italy,
[5]Consorzio RFX, Associazione EURATOM/ENEA sulla Fusione, Padova, Italy,
** See annex of J. Pamela et al, "Overview of Recent JET Results and Future Perspectives", Fusion Energy 2002 (Proc.□/19th IAEA Fusion Energy Conference, Lyon (2002)).*

ABSTRACT

Experiments on JET with ICRH acceleration of neutral beam ions allows to create plasma conditions with a large population of energetic ions in the MeV range. The scope of these experiments is to study various aspects of fast particle physics relevant to burning plasmas. In addition, it is possible to test new diagnostic techniques for fast particles. We report on measurements of escaping MeV ions losses performed during recent Helium plasma experiments with ICRH third harmonic acceleration of Helium beam ions. The measurements are based on activation technique. Samples made of suitable materials, inserted inside the vacuum vessel and located near the plasma edge, are used as flux monitors. Activation due to fast neutrons with $E_n > 2.5MeV$ is observed. Activation caused by losses of alpha particles is found below detection limit. However, significant activation due to losses of protons and deuterons is observed. To enhance the sensitivity of the analysis, a dedicated technique was applied to obtain activation measurements with very low background. Exposed sample surfaces are contaminated with various materials sputtered from the sample holder or the machine walls. This effect is discussed and can in some cases make the interpretation of measurements more difficult. Combining activation data with additional surface analysis data (SIMS), it is possible to assess angular distribution of measured fast particles. Counter-going fast ions are recorded, mainly, and with a local pitch angle in the range of $-0.6 < \xi < 0$ in agreement with fast particles trajectory calculations.

1. INTRODUCTION

The detection of both slowing down and escaping alpha particles remains one of the crucial and most delicate issues in reactor grade plasmas. The lack of established techniques to measure these particles has been recognized as one of the diagnostic weakness of the tokamak community, requiring further R&D in the perspective of ITER. In JET a series of methods are being developed to measure the slowing down alphas. These approaches involve different experimental techniques, ranging from neutron spectrometry and γ-ray and Extreme Ultraviolet spectroscopy to Neutral particle Analysis. On the contrary, at the moment no diagnostic is available to measure the alpha particle losses. For JET-EP two new systems, using Faraday cups and organic scintillators, are going to be installed to overcome this deficiency. Unfortunately both sensors are intrinsically incapable of distinguishing the alphas from the fast deuterons. The present note describes an approach, based on the activation technique, with the potential of resolving the contribution of the lost α from other fast ions. The measurement is based on the activation technique. A thin target material is activated under MeV alpha particles bombardment and isotopes are produced from reactions of type (α, p) , (α,n) , (α,γ). The isotope product has a well-known decay γ ray line. Therefore the measurement of the decay γ ray line is a direct measurement of the dose of alpha particles received by the target. The γ-rays being the result of a nuclear reaction decay, their energy identifies the particle striking the target, allowing discrimination between α and fast

deuterons or other fast ion species. Only ions with sufficient energy,i.e above the energy threshold of the nuclear reaction, are recorded. The first test measurements, performed during the Reversed Field Campaign in May 2003 are reported in [1]. A new instrument with a dedicated design has been manufactured recently at JET and made available for 'alpha particle simulation experiments' in the last campaign C14 before the planned 2004 shutdown. In these experiments alpha particles with energies beyond MeV level are generated with ICRF heating. The paper is organized as follows: First, experiments are described in section 2. The new activation probe is described in section 3. In section 4, experimental results are presented. In section 5, these results are discussed and compared with calculations. Conclusions are summarized in the last section.

2. ALPHA PARTICLE SIMULATION EXPERIMENTS

During JET experiments with ICRH third harmonic heating of ^4He beam ions, the 4.4 MeV γ radiation due to the first excited state of ^{12}C has been observed. Acceleration of ^4He beam ions above an energy of 1.7 MeV is required for this reaction to occur. In these discharges the density is rather low ($n_e \simeq 3.10^{19} m^{-3}$). Magnetic field is 2 T and plasma current 2 MA. The beam energy is 110 keV, the ICRH frequency is 51 MHz and the ICRH power needs to be sufficiently high($\geq 6MW$). Beryllium evaporation is needed before experiment to obtain a sufficiently high Beryllium impurity concentration required to produce enough $Be(\alpha, n\gamma)C$ nuclear reactions. It is then possible to study a large population of high energy alpha particle in this scenario with no need to fuel Tritium in the discharge. Alpha particle simulation experiments were performed successfully in about 30 discharges, during February 2004 . The main gas in the vacuum chamber is Helium. But in some discharges, the deuterium concentration can reach 50 %. Evidence of large populations of alpha particles and deuterons above MeV level is seen from the neutron and gamma ray spectroscopy from nuclear reactions $^9Be(\alpha, n\gamma)^{12}C$, $^{12}C(d, p\gamma)^{13}C$. A typical gamma ray spectrum is shown in figure 1. It must be noted that the peak at 4.4 MeV can result not only from reaction of α particles with Beryllium but also from the other following reactions: 1) C(n,n') neutron inelastic scattering on Carbon 2) (C(p,p')C - proton inelastic scattering on Carbon 3) (C(d,d')C - deuteron inelastic scattering on Carbon and finally another reaction involving Beryllium and Helium3 can also produce 4.4 MeV gamma rays. Therefore caution is needed for the interpretation of the 4.4 MeV peak.

3. ALPHA PARTICLE ACTIVATION PROBE

A skecth of the new fast particle activation probe is shown in figure 2. The probe body is made of Boron Nitride. Boron Nitride has excellent thermal and mechanical properties and it is suitable for use inside the vacuum chamber. Samples are installed into 6 slots having a different orientation. With several slots having different orientations, the local pitch angle distribution can be resolved. Several samples are installed in each slots with different materials having different nuclear reactions with fast ions and different thresholds. This allows to discriminate between different ion

species and have some spectrum information. There are 18 samples exposed with a thickness of 1mm. 6 samples are installed at the back in a shielded location.

Material	Number of samples	Typical size	Mass
Natural Ti	6	10mm X 10mm	0.45 g
MgF_2	6	10mm X 10 mm	0.315 g
TiAlV	6	30mm X 10 mm	1.35g

3.1. PROBE LOCATION

The activation probe is installed at the lower end of a 40mm diameter manipulator arm. The manipulator arm has an access vertically downwards inside the JET vacuum vessel through a 'slit shaped' port as shown in figure 3.

3.2. SAMPLES ORIENTATION

Sample orientations are shown in figure 4. Two of the sample containing slots (slots 1 and 4) have their orientation in the perpendicular or poloidal plane. Local losses of fast ion are highly anisotropic. Trajectory calculations show that a purely perpendicular fast ion velocity distribution, for example, would result on recording fast ions only on samples inserted into slot 1 (the slot pointing to inward radial direction).

3.3. SAMPLES COMPOSITION

The material inventory comprises 5 different elements (Z) and 12 different isotopes (A):

Isotope	Abundance	Number of atoms
Titanium 46	8.25%	22.0410^{21}
Titanium 47	7.44%	19.8710^{21}
Titanium 48	73.7%	196.910^{21}
Titanium 49	5.5%	14.710^{21}
Titanium 50	5.2%	13.910^{21}
Vanadium 50	0.25%	0.009 10^{21}
Vanadium 51	99.75%	13.89 10^{21}
Magnesium 24	79%	14.4 10^{21}
Magnesium 25	10%	1.83 10^{21}
Magnesium 26	11%	2.01 10^{21}
Fluorine 19	100%	36.5 10^{21}
Aluminium 27	100%	10.9 10^{21}

4. OBSERVED GAMMA SPECTRA

4.1. SPECTRAL LINES OF INTEREST

In the table below, we display the gamma ray radiations of interest that originate from reactions between fast ions and sample materials. We indicate also the neutron-induced reactions. They are listed according to the energy of gamma ray radiation emitted. In the last column, we indicate whichever spectral lines have been observed on the samples . If the line is not observed, a value for the sample activity in milli-Becquerel, called ’decision threshold’ is indicated instead which has the following de£nition: there is a 5% probability that the activity quoted could not have been detected, or there is 95% con£dence that the real activity of the sample is below this value.

Energy(MeV)	Isotope	Half life	Reaction	Detection limit (mBq)
0.112	Cr48	21.6h	He3 on Ti	-
0.159	Sc47	3.35d	Ti47(n,p)Sc47	observed
0.175	Sc48	1.82d	Ti48(n,p)Sc48	traces
0.271	Sc44	2.4d	He3 on Ti	-
0.320	Cr51	27.7d	α on Ti	< 4
0.835	Mn54	312d	α on V	observed
0.889	Sc46	83.8d	Ti46(n,p)Sc46	observed
0.983	Sc48	1.82d	Ti48(n,p)Sc48	observed
0.983	V48	15.97d	Ti48(p,n)V48	< 0.5
1.037	Sc48	1.82d	Ti48(n,p)Sc48	observed
1.12	Sc46	83.8d	Ti46(n,p)Sc46	observed
1.157	Sc44	2.4d	He3,D on Ti	traces
1.274	Na22	2.6y	α on F	< 0.14
1.312	Sc48	1.82d	Ti48(n,p)Sc48	observed
1.312	V48	15.97d	Ti48(p,n)V48	< 0.5
1.368	Na24	15H	n, He3 on Mg	observed
2.240	V48	15.97d	Ti48(p,n)V48	out of range
2.754	Na24	15H	n,He3 on Mg	out of range

4.2. SPECTRAL LINES FROM NEUTRON ACTIVATION

Neutron-induced reactions which are observed are shown in figure 5 and are also listed in the table below:

Reaction string	Energy threshold(MeV)
Ti47(n,p)Sc47	1.
Ti46(n,p)Sc46	3.
Ti48(n,p)Sc48	5.
Mg24(n,p)Na24	5.5
Al27(n,p)Na24	5.4

Scandium46 line comes mainly from the reaction Ti46(n,p)Sc46. The count rate observed is compatible with the total neutron yield measured with the fission chamber. Scandium47 line at energy of 159 keV comes mainly from reaction Ti47(n,p)Sc47. The count rate is also compatible with the total neutron yield. The Sc48 lines respectively at energy of 1037, 983 and 1312 keV comes mainly from reaction Ti48(n,p)Sc48. The threshold for this reaction is 5 MeV revealing energetic neutrons above this value. The activation measured with this reaction agrees well with

the activation measured with ^{24}Na peak, the last 2 reactions. This confirms the detection of fast neutrons with energy above E_n ¿ 5 MeV.

By combining the information from all these lines it is possible to obtain an estimation of the neutron spectrum. The spectrum is time-integrated over the total duration of sample exposure. The spectrum plotted in figure 6 shows fast neutrons with $E_n > 2.5MeV$ produced at an identical rate than less energetic neutrons. But at energy above 5 MeV , the spectrum falls at a few percent. A similar neutron energy spectrum has been measured with another diagnostic.

The error in the spectrum comes mainly from statistics and is around 20% for the Na24 peak. As it is a relative measurement the systematic error is excluded. No unfolding procedure has been used.

The above spectrum was obtained with the assumption that the observed radionuclides are produced only from neutron-induced reactions. For example, deuterons above 6.9 MeV can produce Sc46 via the reaction $^{48}_{22}Ti(D,\alpha)^{46}_{21}Sc$ and deuterons above 3 MeV can produce Sc48 with reaction $^{50}Ti(d,\alpha)$. Sc46 is found on the back samples which are shielded from charged particles. The production is therefore primarily from neutron activation.

4.2.1. Angular distribution for ^{46}Sc

Figure 7 shows the angular distribution for ^{46}Sc radionuclides. The orientation angle is counted clockwise from the direction of the toroidal magnetic field,i.e the angle with slot 1 is 90 degree. The local neutron irradiation condition is expected to be isotropic on the scale of the probe dimension. Measurements show surprisingly that the angular distribution of radionuclides on the samples is not uniform, revealing an anisotropy in the incident neutron flux for fast neutrons with energy $E_n > 3MeV$. Angular distribution measured by both set of samples agree qualitatively in shape with a generally higher flux measured with T samples. There is an increased level (maximum) of activation for both samples looking at the inward and outward radial direction, i.e at 90 deg and -90 deg with respect to the direction of toroidal field. A possible explanation is a highly anisotropic neutron emission during ICRH experiments. Both reactions $D(d,n)^3he$ and $Be(\alpha,n)C$ have anisotropic differential cross-sections. Figure 8 shows the increase with energy in angular dependence of the $D(d,n)^3he$ reaction. Other possible explanations may be, parasitic sources of Sc46 and sources of fast neutrons located at sample surface.

4.3. OTHER SPECTRAL LINES

4.3.1. Ultra low level gamma ray spectroscopy technique

In the spectrum shown above in figure 5, gamma ray lines have very low intensities. The measurement, however, was taken with all samples and holder together. Due to the very low activity of our samples we are reaching the sensitivity limit of the detector systems which are available on site at JET. To investigate the emission of each individual sample and find signature of lost alpha

particles we had to go to higher sensitivity measurements. For the first time, we used a special low background technique which main features are

- Underground laboratory
- Highly efficient detectors
- Detector system and shielding made of selected radiopure elements

In order to measure very weak activity it is necessary to measure underground. Measurements above ground suffer from the fact that highly energetic radiation interferes with detectors and create non-desirable background. We gave our samples for analysis to the IRMM Institute for Reference Materials and Measurements. This institute operates several high purity Germanium detectors in a special underground laboratory facility called HADES. It is located 223m below sea level at Belgian Nuclear Research center (SCK-CEN). Figure 9 shows the gain of 3 order of magnitude which is achieved in the background reduction:

The spectrum in figure 10 is a measurement of the TitaniumAluminumVanadium sample with orientation viewing the inward radial direction.

Beside scandium isotopes discussed previously, following radionuclides are found on the sample: Mn-54, Be-7, Co-57, Co-56. It must be noted that only Mn-54 can be produced from a reaction with the sample material. Figure 11 shows the angular distribution for Mn-54. This distribution is rather different than the one of figure 7.

Be-7, Co-56, Co-57, Co-58 can be transported directly on the sample or originate from reactions with material transported on the sample surface. All exposed samples contain some radionuclides which are transported materials. The shielded samples at the back of the holder do not contain these elements. This is an indication that they are not produced from neutron or gamma irradiation. Figure 12 shows the angular distribution for Co-58

Figure 13 shows the angular distribution for ^{7}Be.

4.3.2. Mn-54

The origin of Mn-54 is ambiguous. It can come both from alpha particle bombardment on Vanadium or from neutron activation of Fe-54. It is not possible to exclude or separate the two contributions. However the fact that it is also found on the pure Titanium sample indicate it is more likely to be a deposited material. In addition, it is not consistent with the absence of Na-22 on Fluorine samples.

4.3.3. Co radionuclides

Cobalt radionuclides originate from nuclear reactions on Ni and Fe, which are main elements entering the composition of the vacuum vessel. Angular distribution for Co58 is shown in figure 13.

4.3.4. Be-7

Be7 angular distribution is shown on figure 13.Be7 can be produced as result of nuclear reaction of protons and deuterons with Boron.

5. DISCUSSION OF EXPERIMENTAL RESULTS

5.1. PREDICTION OF FAST ION LOSSES

We discuss here fast ion classic drift losses or prompt losses only as it is the dominant loss mechanism in discharges with plasma current ≤ 3 MA[2, 5]. Classic drift losses are calculated with the MCorbit Monte Carlo Code[3]. The MCorbit Monte Carlo Code is designed to follow the trajectories of many particles (up to several ten thousands) and compute the fraction of unconfined orbits in the JET D-shape geometry . It can use the equilibrium magnetic field given by EFIT. It does not take into account field ripple which is weak at JET. The MC orbit code can also use the actual birth spatial profile of the fast ions as seen from the 19 channels profile monitor. It can also resolve the losses distribution at the wall poloidally but not toroidally. The vessel walls geometry is not incorporated in full details but a typical section is used instead. Figure 14 shows a typical case for the dependence of prompt losses as function of flux surface coordinate ψ. Most losses occur evidently close to the edge. Figure 15 shows the poloidal location of impact of fast ions at the wall. It can be seen that with the clockward standard orientation of toroidal magnetic field (looking at the torus from above) the detector is located in a region of weak losses, but the losses do not vanish completely at the detector location. With reversed field, the poloidal fraction of losses at detector location can reach a few $\%$ while only of the order of 10^{-4} for standard field. Figure 16 and 17 give a typical result of a simulation for the quantitative prediction of spatial distribution of lost fast ions at the wall. Figure 18 shows the local pitch angle distribution at impact. It is interesting to note that most of fast ions hit walls with pitch angle close to 90 degree and that mostly counter-travelling ions are lost in the upper part of the vacuum vessel whereas it is the opposite in the lower part of the vacuum vessel.

5.2. RESULTS FOR ALPHA PARTICLE LOSSES

Mainly 3 nuclear reactions were used to monitor the flux of escaping α particles at detector location. The results are listed in the table below:

Reaction	Results
${}^{19}_{9}F(\alpha,n)^{22}_{11}Na$	α particles flux $\leq$ 1.e+11 cm-2 with $E_\alpha \geq 2.6MeV$
${}^{48}_{22}Ti(\alpha,n)^{51}_{24}Cr$	α particles flux$\leq$ 1.e+12 cm-2 with $E_\alpha \geq 4MeV$
${}^{51}_{23}V(\alpha,n)^{54}_{25}Mn$	α particles flux $\simeq$ 1.e+11 cm-2 with $E_\alpha \geq 4MeV$

$^{54}_{25}Mn$ has been detected on the samples. $^{22}_{11}Na$ and $^{51}_{24}Cr$ have not been observed and are below the detection limit. Measurements indicate mainly 2 things: 1) alpha losses are very low: we are close to or below the detection limit 2) at very low level of activation deposition of material is a possible non negligible contribution. Therefore, there is a need in the future to be able to separate transported material and direct activation of samples. It would then be possible to distinguish whether $^{54}_{25}Mn$ is produced by incident alpha particles or transported directly onto the sample surface. Another option is to select, when possible, a radionuclide which has no other source or does not build-up in the machine.

5.3. SURFACE ANALYSIS OF SAMPLES

In order to investigate the contamination of sample surfaces, we performed standard Secondary Ion Mass Spectroscopy (SIMS) measurements using the ToF-SIMS apparatus at Forschungzentrum Juelich, Germany. An oxygen atomic beam at an energy of about 2 keV is projected onto the sample surface and the sputtered particles are analyzed. SIMS analysis for TiAlV sample number 1 is shown in figure 19. It shows that the surface layer of the TiAlV sample contains the following 'contaminating' elements:

- Boron
- Beryllium
- Carbon
- Iron

Boron, likely, comes from the sputtering of the BoronNitride sample holder. Carbon and Beryllium are relatively important impurity elements inside the vacuum vessel. Beryllium evaporation was also applied before experiment. Iron is sputtered from the vessel walls. Interestingly, these elements are found on all samples and they are not necessarily distributed uniformly between the samples as shown in figure 20 below for the case of Boron10:

The density of Boron10 layer is the highest on sample 2. The layer thickness is estimated between 500nm and 2μm.

5.4. BE7 CONTAMINATION ON SAMPLE SURFACES

The existence of ^{7}Be radionuclides on the sample surfaces is due to several mechanisms of which, we give a list below of the most likely ones:

- A background source of ^{7}Be exist inside the machine. The ^{7}Be background can then be sputtered and a fraction of it transported onto the sample surfaces. In that case, the observed ^{7}Be angular distribution should be similar to a material deposition pattern

- The sample holder, containing Boron is activated and ^7Be is produced. A fraction of ^7Be is then transported onto the sample surfaces
- ^7Be is produced on the sample surface due to activation reactions with the thin boron coating on the sample surface. In that case, the observed ^7Be angular distribution should be similar to the distribution of fast particles

Possibly, all 3 mechanisms give a contribution at some degree. However, assuming that the third mechanism is the dominant one and that both others contribute significantly less, we find that the experimentally measured absolute amount of ^7Be and its angular distribution agrees better with the calculations.

5.5. LOSSES OF FAST DEUTERONS AND PROTONS AND ASSESSMENT OF ANGULAR DISTRIBUTION

The absolute amount of ^7Be measured on the sample surfaces requires a time-integrated local fast particle flux (deuterons and protons) at detector location in the range of $10^{13} - 10^{14} cm{-}2$, assuming that it is produced dominantly by activation of the thin boron film covering the sample surface. Combining activation data with additional surface analysis data (SIMS), it is possible to assess angular distribution of measured fast particles. Counter-going fast ions are recorded, mainly, and with a local pitch angle in the range of $-0.6 < \xi < 0$ in agreement with trajectory calculations.

Angular distribution of the fast particle flux is shown in the figure 21 below:

6. CONCLUSION AND NEXT STEPS

In recent JET experiments (February 2004) with fast ions in Helium plasmas, in-vessel samples were used as flux monitors for escaping fast particles. A variety of radionuclides due to activation reactions are found in the samples. Some of these radionuclides are produced as a result of neutron activation. A neutron energy spectrum can be inferred from the measurements and show that neutron emission is rather flat as function of energy between 1 MeV and 5 MeV and then falls at an energy above 5 MeV. This result is in agreement with other measurements of the neutron spectrum. Activation caused by losses of MeV alpha particles is found below the detection limit. Activation due to losses of MeV protons and deuterons is observed. For the first time, we used a special technique for the measurement of low level activation called ' Ultra low level gamma ray spectroscopy'. Exposed sample surfaces are contaminated with various materials sputtered from the sample holder or the machine walls. This effect can in some cases make the interpretation of measurements more difficult. Two processes occur simultaneously: 1) activation of sample material and 2) the transport of material which modify the composition of the sample surface. Combining activation data with additional surface analysis data (SIMS), it is possible to assess angular distribution of measured fast particles. Counter-going fast ions are recorded, mainly, and

with a local pitch angle in the range of $-0.6 < \xi < 0$ in agreement with fast particles trajectory calculations.

7. FUTURE WORK

Several options exist for future experiments to explore the potential of activation technique as a diagnostic for lost fast particles. These options depend on, essentially the detector position and the orientation of toroidal field. In the current setup, the detector is located in a region of weak losses when the tokamak is operated with the standard orientation of the magnetic field. If experiments are repeated in the same conditions (i.e same detector position and toroidal field), we need to cover the samples with a thin foil, for example 1 micron gold or tungsten foil. This will allow to separate a possible contribution from deposited materials. But, this can be technically difficult. Protons and deuterons could be measured. To measure alpha particles would require to enhance the sensitivity, for example, by using larger size fluorine samples. Preparation of nuclear targets with ion implantation technique should be explored. The best option, however, is to have experiments with reversed toroidal field and which the losses of MeV ions at detector location are increased by several orders of magnitude. A good scenario is the ICRF minority heating of ^3He in Deuterium plasma in order to produce simultaneously high energy protons and alpha particles through the fusion reaction $d(^3He, p)\alpha$. This is an excellent scenario to demonstrate the capability of the diagnostic technique to measure simultaneously different fast particle species.

ACKNOWLEDGEMENTS

The authors gratefully acknowledge the support and contribution made directly and indirectly by members of plasma boundary group, including M. Stamp, G. Matthews, J. Vince and G. Kaveney. This work was carried out under the European Fusion Development Agreement.

REFERENCES

[1] G. Bonheure et al *First MeV ion losses measurements using activation technique in reversed B experiments at JET, Review of Scienti£c Instruments, vol75n10,p3540, October 2004*

[2] Y. I. Kolesnichenko *The role of alpha particles in tokamak reactors, Nuclear Fusion, Volume 23 N10,730(1980)*

[3] G. Sadler, P. Van Belle, M. Hone, N. Jarvis, J. Kallne, G. Martin and V. Merlo *Fusion product measurements on JET, Proceeding of 13th EPS conference in Schliersee, Vol10C,105(1986)*

[4] S. Conroy, N. Jarvis, G. Sadler, M. Huxtable *Time resolved measurements of Triton burnup in JET plasmas, Nuclear Fusion, Volume 28 N1,2127(1988)*

[5] G. Bonheure et al *Report on the Escaping MeV ion losses measurements based on Activation technique during C9 JET campaign, JET internal report EFDA-JET-R(03)01 (2003),2*

[6] H.Liskien, A. Paulsen *Neutron production cross sections and energies for the reactions* $T(p,n)^3He$*,* $D(d,n)^3He$ *and* $T(d,n)^4He$*, Nuclear Data Tables 11,569 (1973)*

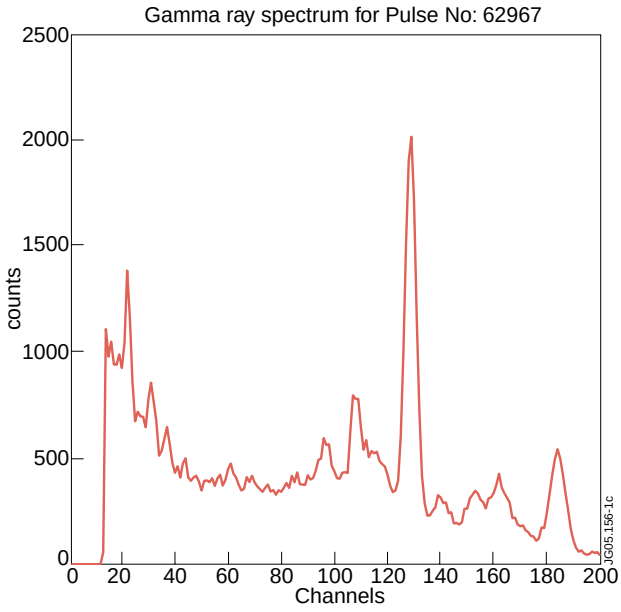

Figure 1: Gamma-ray spectra from discharge 62957 time-integrated over the full discharge. Peaks at 3.09 and 4.4 MeV are emitted due to $^{12}C(d, p\geq)^{13}C$ and $^{9}Be(\pm, n\geq)^{12}C$ reactions

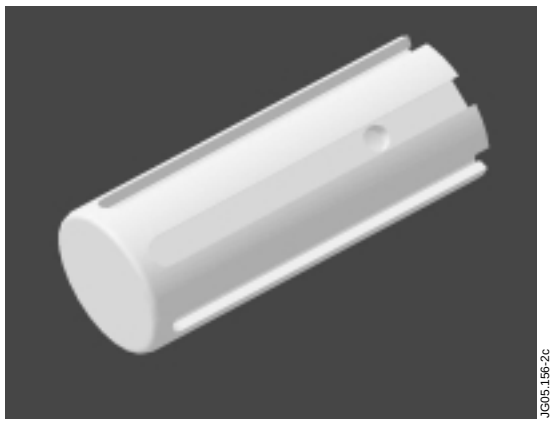

Figure 2: Sketch of the new fast particle in-vessel activation probe: the six samples containing slots are regularly spaced and are 60 degree apart

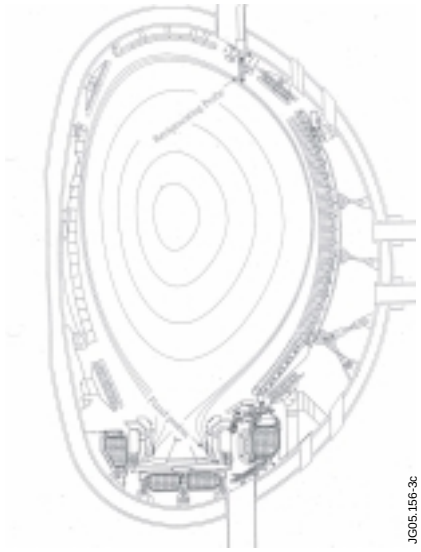

Figure 3: Position of the in-vessel activation probe (marked 'reciprocating probe') shown in the poloidal cross section of the JET torus.

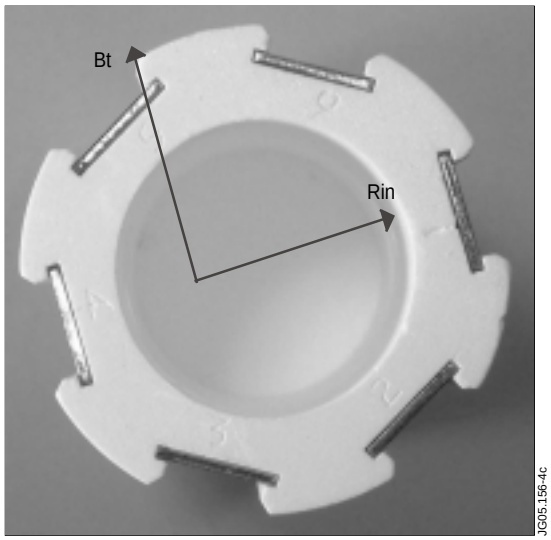

Figure 4: Sample orientations: the six samples containing slots are regularly spaced and are 60 degree apart. Slot numbers are visible on the picture. R_{in} indicates the direction along the major radius and pointing radially inward while Bt indicates the standard direction of the toroidal magnetic field. The orientation angle is counted clockwise from the direction of the toroidal magnetic field, i.e the angle between the toroidal field and slot 1 (R_{in}) is 90 degree.

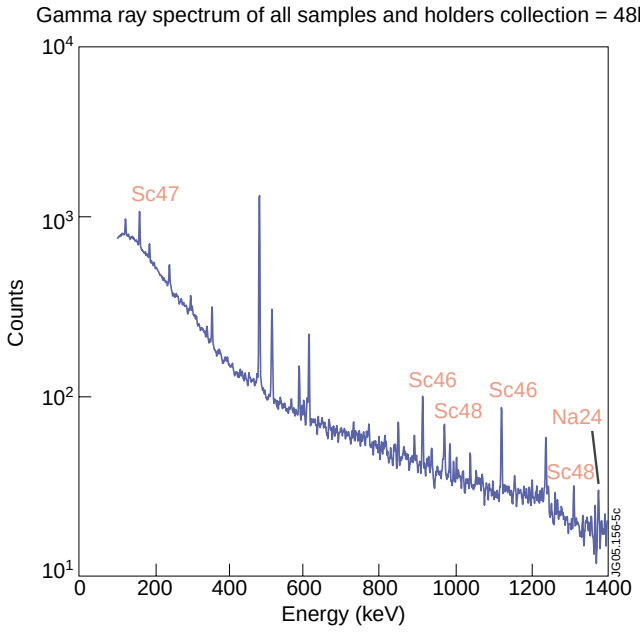

Figure 5: Gamma ray spectrum of all samples and holder: first spectrum collected after experiment.

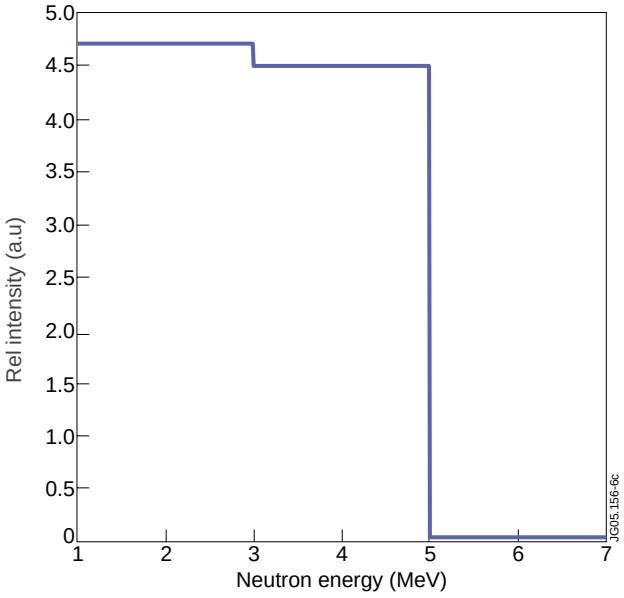

Figure 6: Neutron spectrum deduced from activation of samples

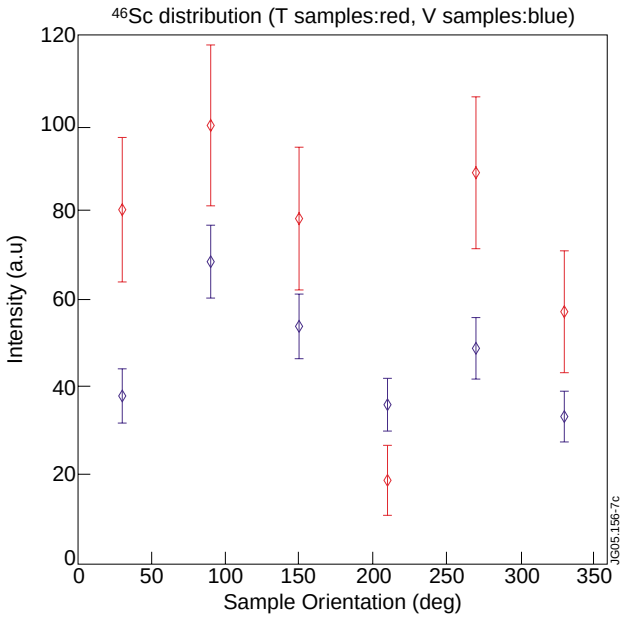

Figure 7: Angular distribution for ^{46}Sc radionuclide from T_i and T_iAlV samples

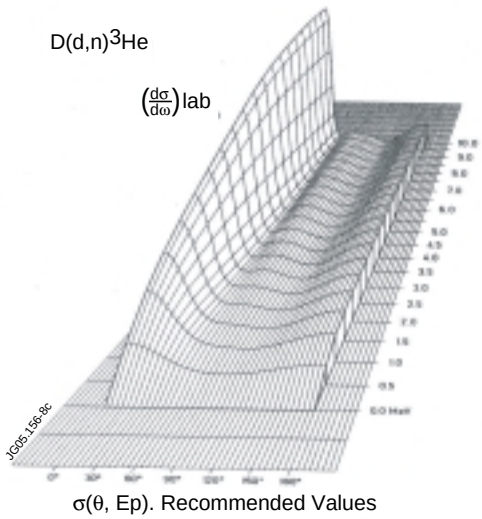

Figure 8: Double differential cross section of D(d, n)^{3}He fusion reaction from reference[6]. Anisotropy increases with fast deuteron energy.

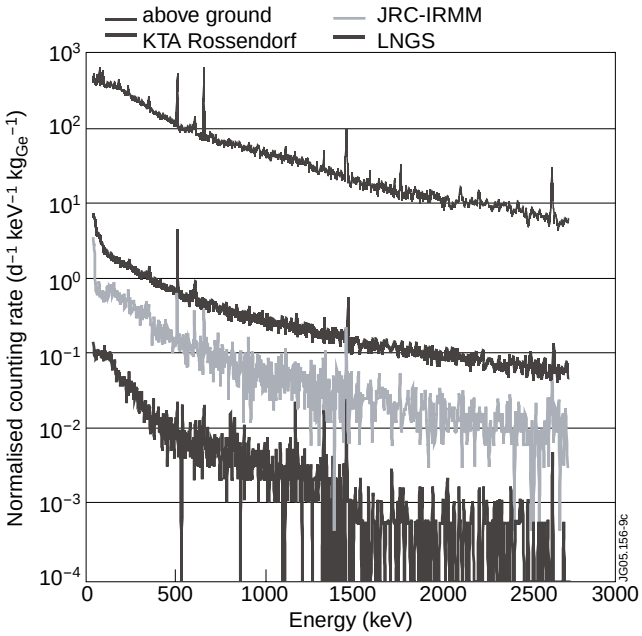

Figure 9: Background gamma ray spectrum measured at various underground laboratory facilities and comparison with groundlevel background. (Courtesy of JRC-IRMM)

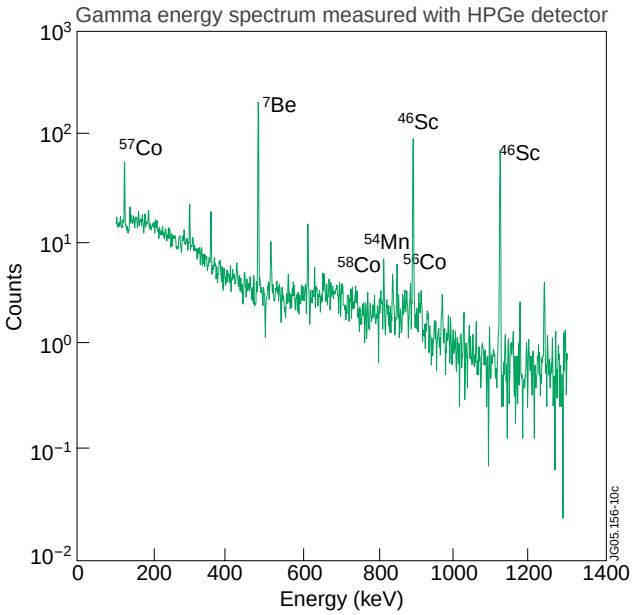

Figure 10: Gamma spectrum from the T_iAlV sample viewing the inward radial direction.

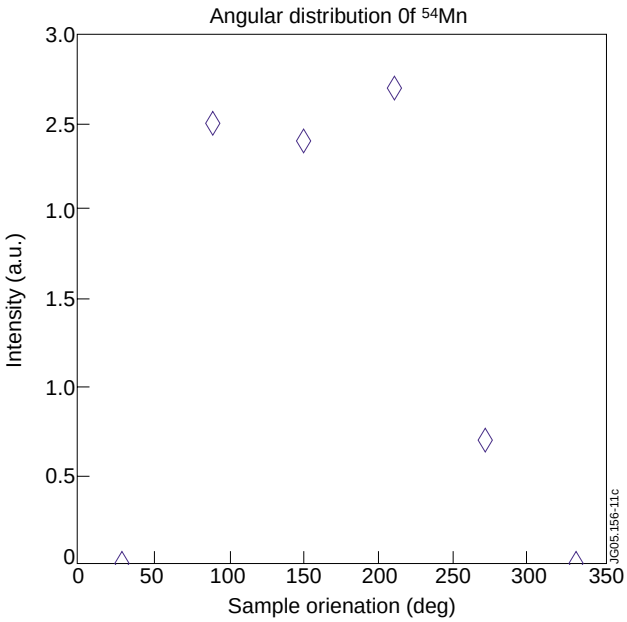

Figure 11: Angular distribution for Mn^{54}

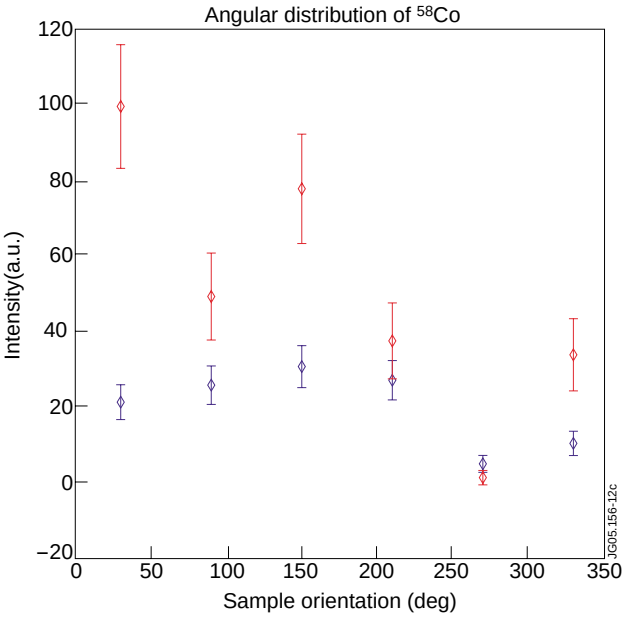

Figure 12: Angular distribution for Co^{58}

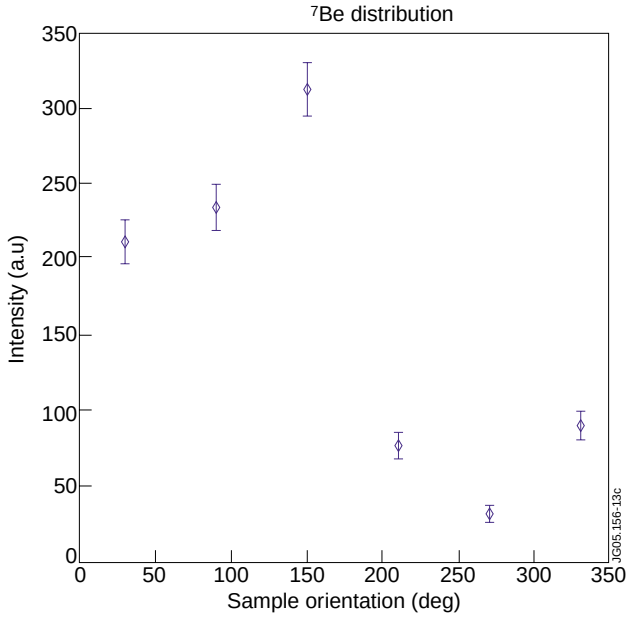

Figure 13: Angular distribution for Be7.

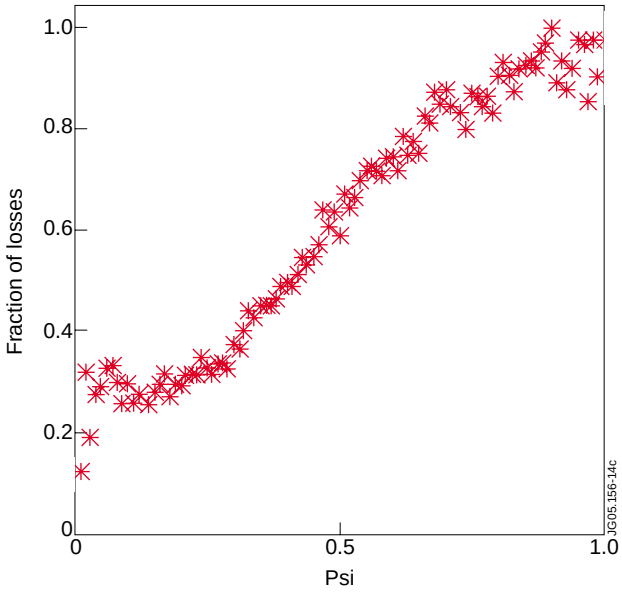

Figure 14: Fraction of losses as function of flux coordinates.

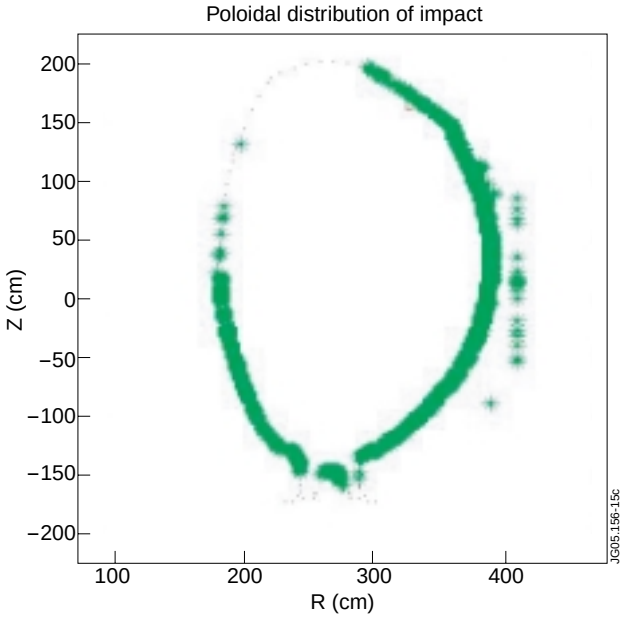

Figure 15: Poloidal distribution of impacts at the wall.

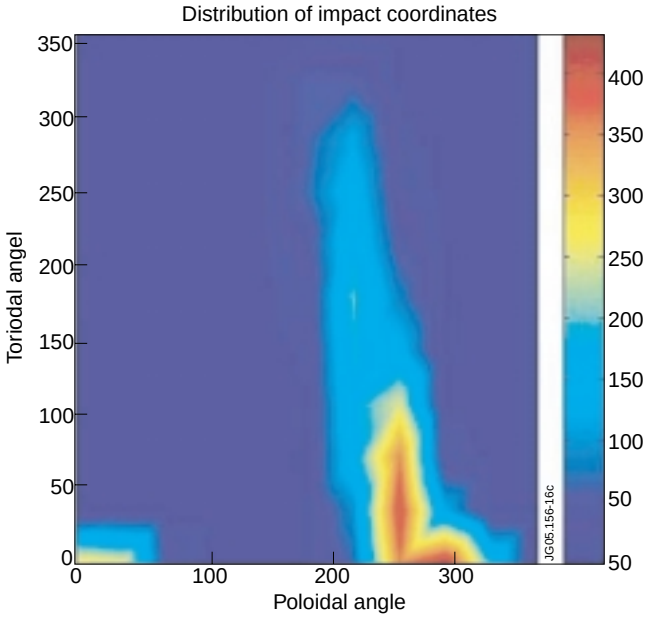

Figure 16: Spatial distribution of losses at the wall - 1) toroidal and poloidal coordinates.

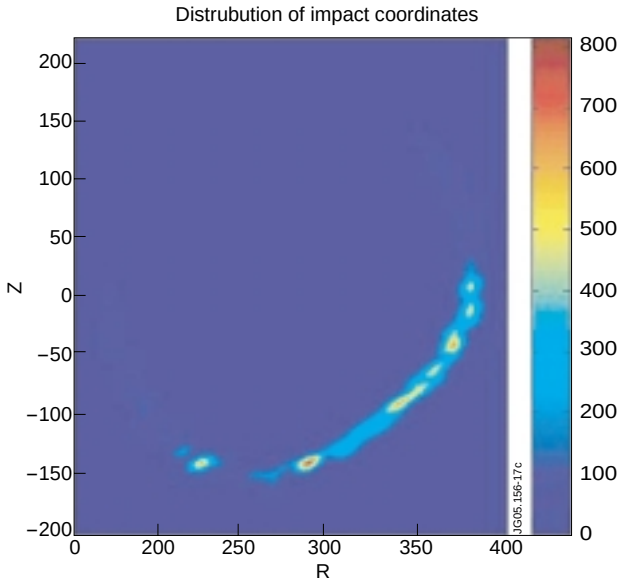

Figure 17: Spatial distribution of losses at the wall - 2) r and z coordinates

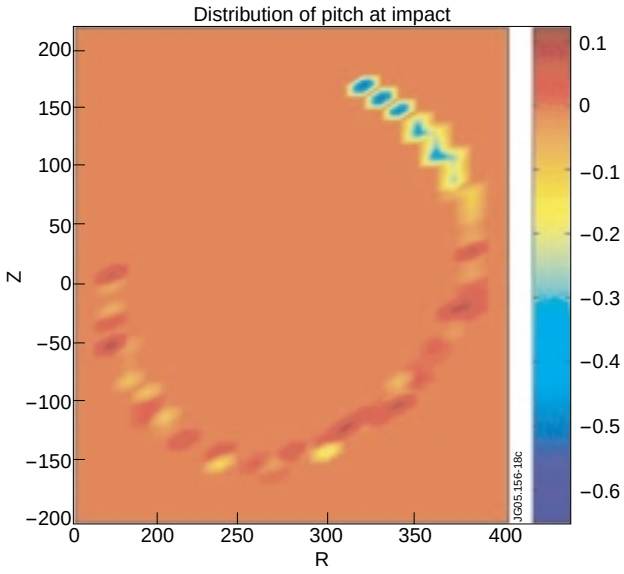

Figure 18: Local pitch angle distribution of losses at the wall

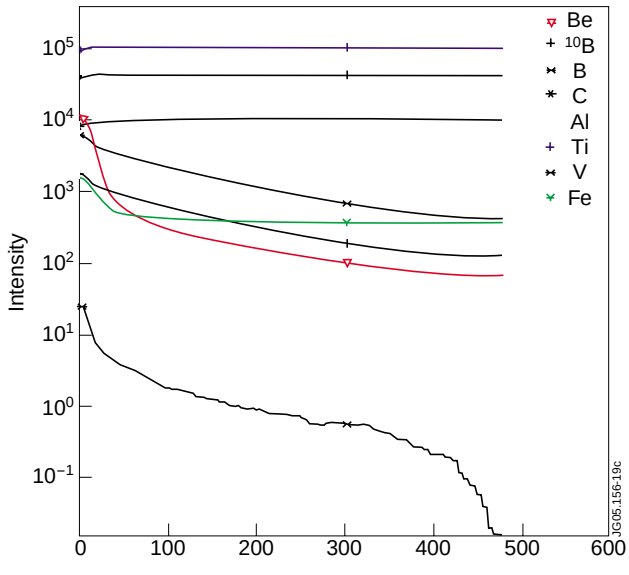

Figure 19: SIMS analysis of the first T_iAlV sample

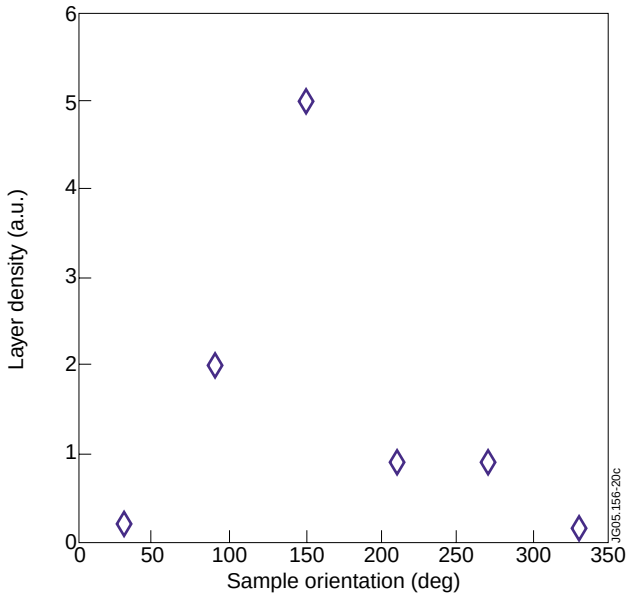

Figure 20: Boron^{10} distribution on the 6 T_iAlV samples

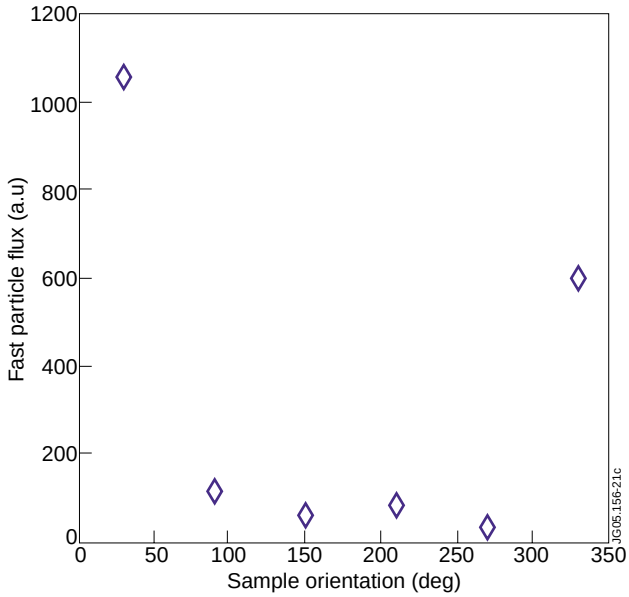

Figure 21: Distribution on the 6 T_iAlV samples of the incident fast particle flux